Supplementary Data

Supplementary Figures

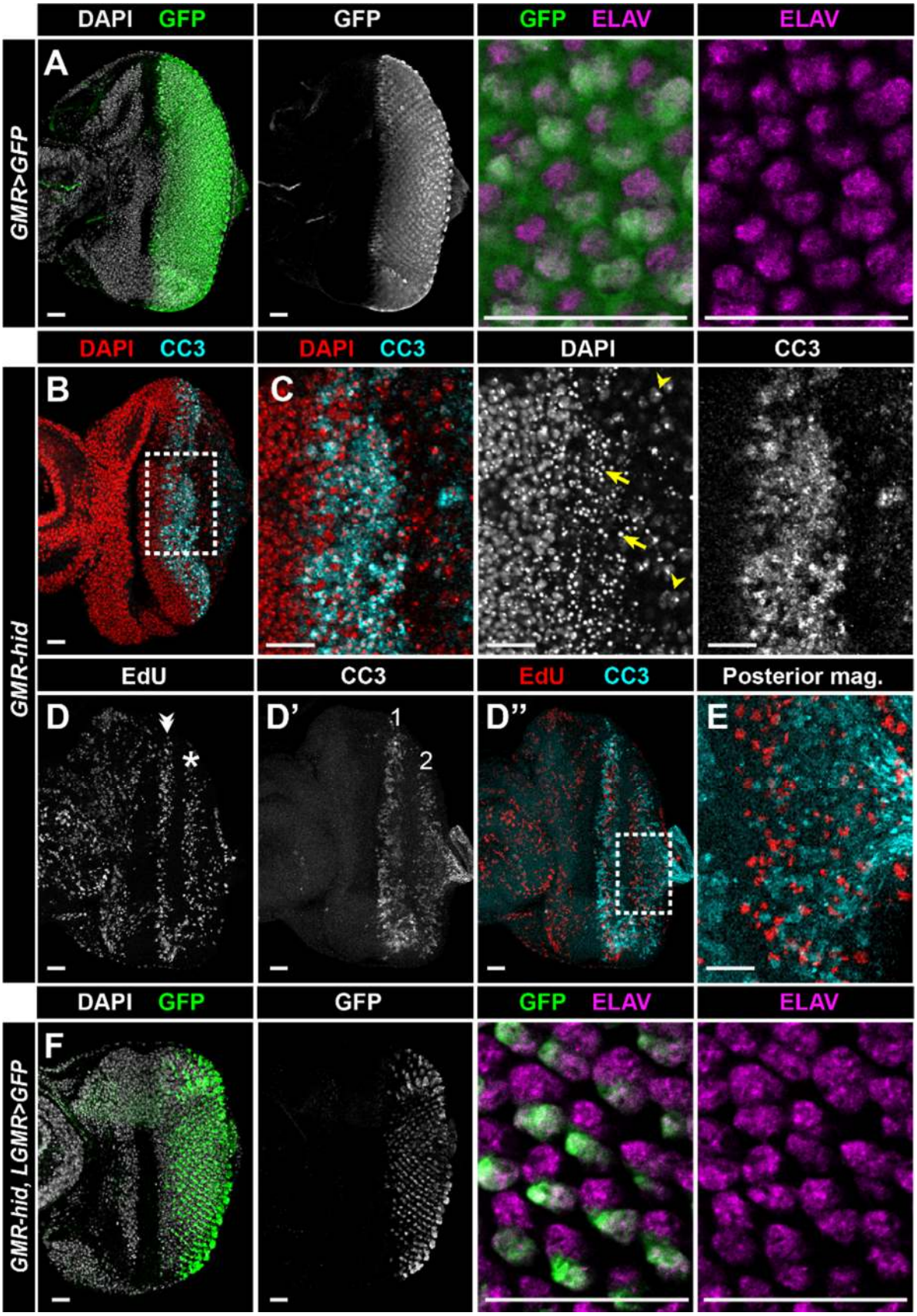

Supp. Figure 1 (related to Fig. 1). Characterization of *GMR-Gal4*, *longGMR-Gal4*, and *GMR-hid* transgenes.

A,F) Expression of GFP (green) driven by *GMR-Gal4* (A) or *longGMR-Gal4* (*LGMR-Gal4*, (F)). Higher magnification of posterior cells in the right two panels indicates photoreceptors stained with ELAV (purple). GFP is expressed in all photoreceptors with *GMR-Gal4* (A) and in a subset of photoreceptors with *LGMR-Gal4* (F).

B-C) DAPI staining of nuclei (red) and staining of apoptotic cells with anti-CC3 antibodies (cyan) on the basal surface of a *GMR-hid* disc. Box in (B) indicates area of magnification in (C). Pyknotic nuclei (arrows) and glial cell nuclei (arrowheads) are present on the basal surface of the disc.

D-E) EdU staining of cells in S-phase (red in D'') in *GMR-hid* discs marks the SMW (double arrowhead) and CP (*). CC3 staining (cyan in D'') marks the two waves of apoptosis (1 and 2). Box in D'' indicates area of magnification in E.

Anterior is oriented to the left. Scale bars: 20 μM.

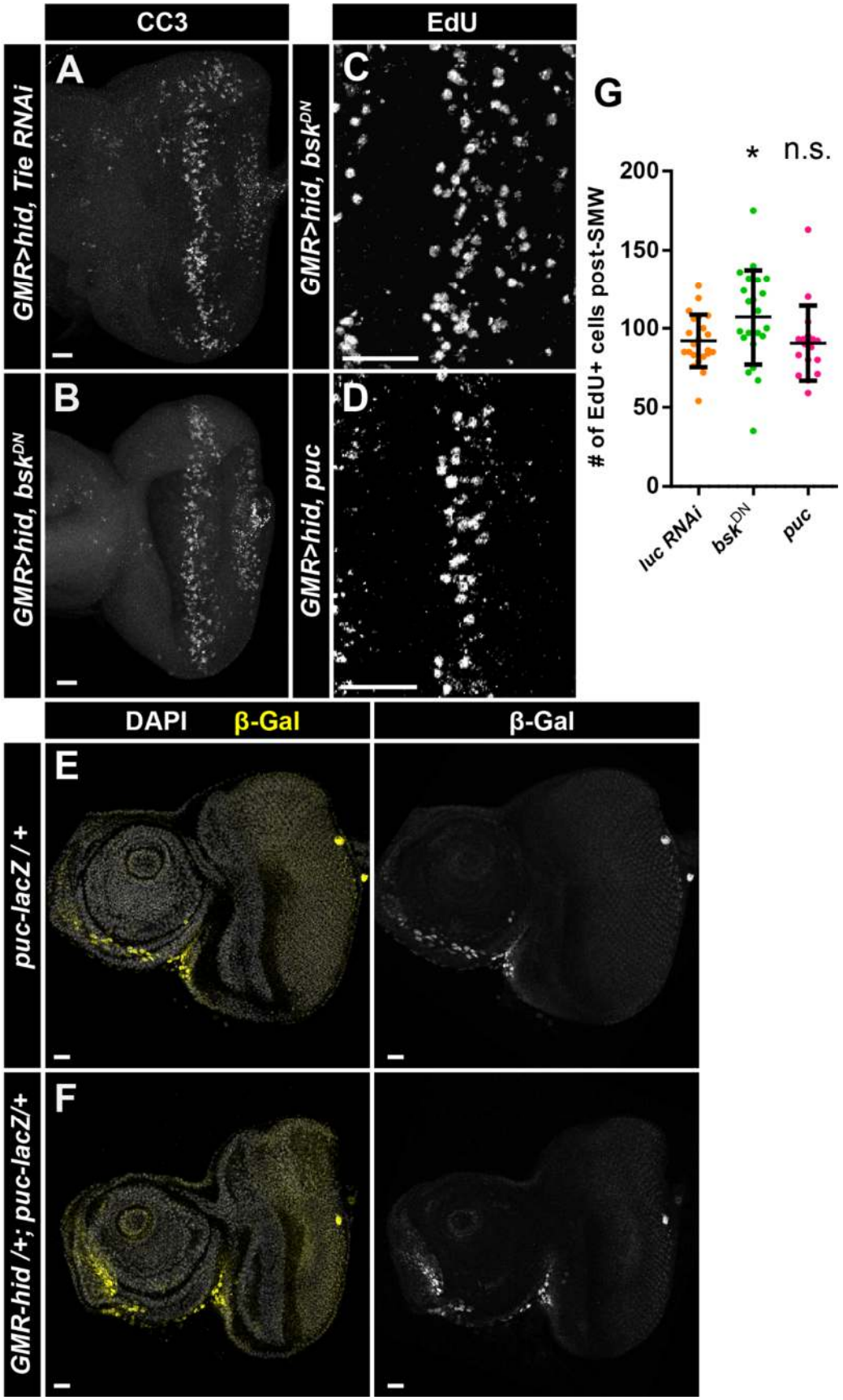
CC3
EdU
A
B
C
D
GMR>hid, Tie RNAi
GMR>hid, bskDN
GMR>hid, bskDN
GMR>hid, puc
G
* n.s.
# of EdU+ cells post-SMW
200
150
100
50
0
luc RNAi
bskDN
puc
DAPI β-Gal
β-Gal
E
F
puc-lacZ / +
GMR-hid /+; puc-lacZ/+

Supp. Figure 2 (related to Fig. 1). Inhibition of signaling through JNK or Tie does not modify the *GMR-hid* phenotype.

A,B) Apoptotic cells stained with anti-CC3 antibodies in the indicated genotypes.

C,D) EdU incorporation in the posterior of eye discs of the indicated genotypes.

E,F) *puc-lacZ* expression, marked by βGal in yellow, is similar in wild type (E) and *GMR-hid* (F) tissues.

G) Quantification of compensatory proliferating cells in the *GMR>hid,Gal4* background for the indicated UAS-transgenes. All post-SMW, EdU^+ eye disc cells were counted. Each circle on the graph represents the number of cells counted for a single disc. For each genotype, $n \geq 17$ discs. Bars represent mean and one standard deviation. n.s., not significant. While *GMR>hid, bsk^{DN}* CP is significantly increased compared to *GMR>hid, luc RNAi* (*P=0.047), it is not significantly different from another control (*GMR>hid, Gal4/CyO*; P=0.43). Therefore, we are wary about drawing conclusions about the biological significance of an increase in CP in *GMR>hid, bsk^{DN}* discs.

Anterior is oriented to the left. Scale bars: 20 μM.

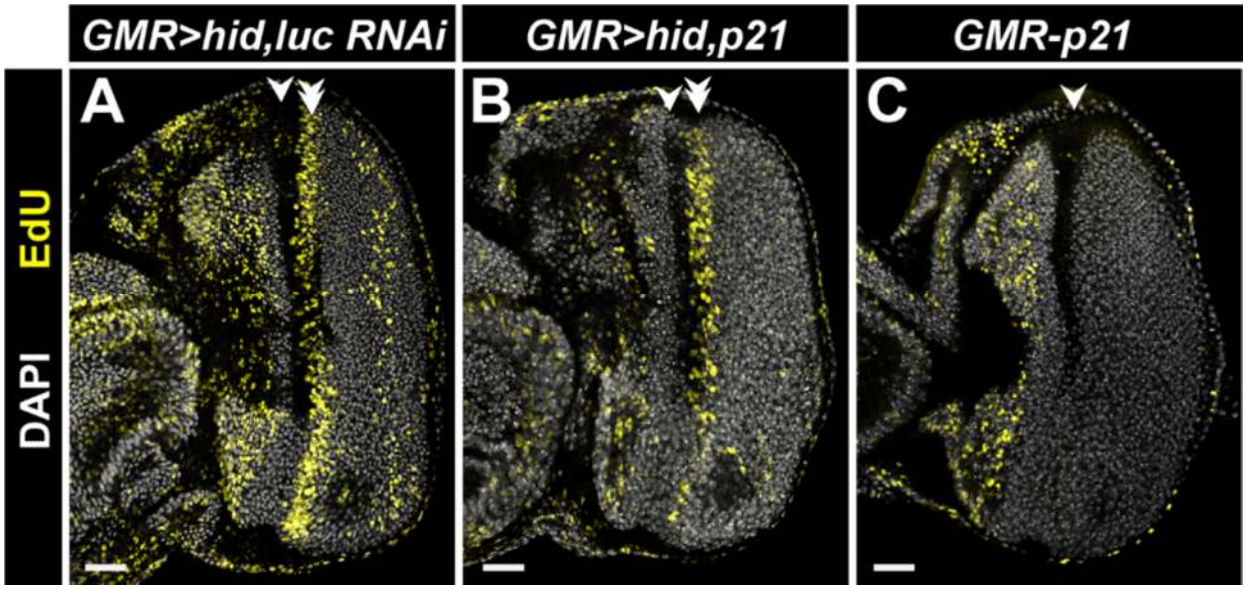

Supp. Figure 3 (related to Fig. 2). Transgenes expressed using *GMR-Gal4* do not affect the second mitotic wave.

A) *GMR>hid, luc RNAi* eye discs stained with DAPI (grey) and EdU (yellow) to indicate MF (arrowhead) and SMW (double arrowhead), respectively.

B) The SMW appears normal when *p21* is expressed with *GMR-Gal4* in the *GMR-hid* background.

C) Expressing p21 via *GMR-p21* results in ablation of the SMW.

Anterior is oriented to the left. Scale bars: 20 μM.

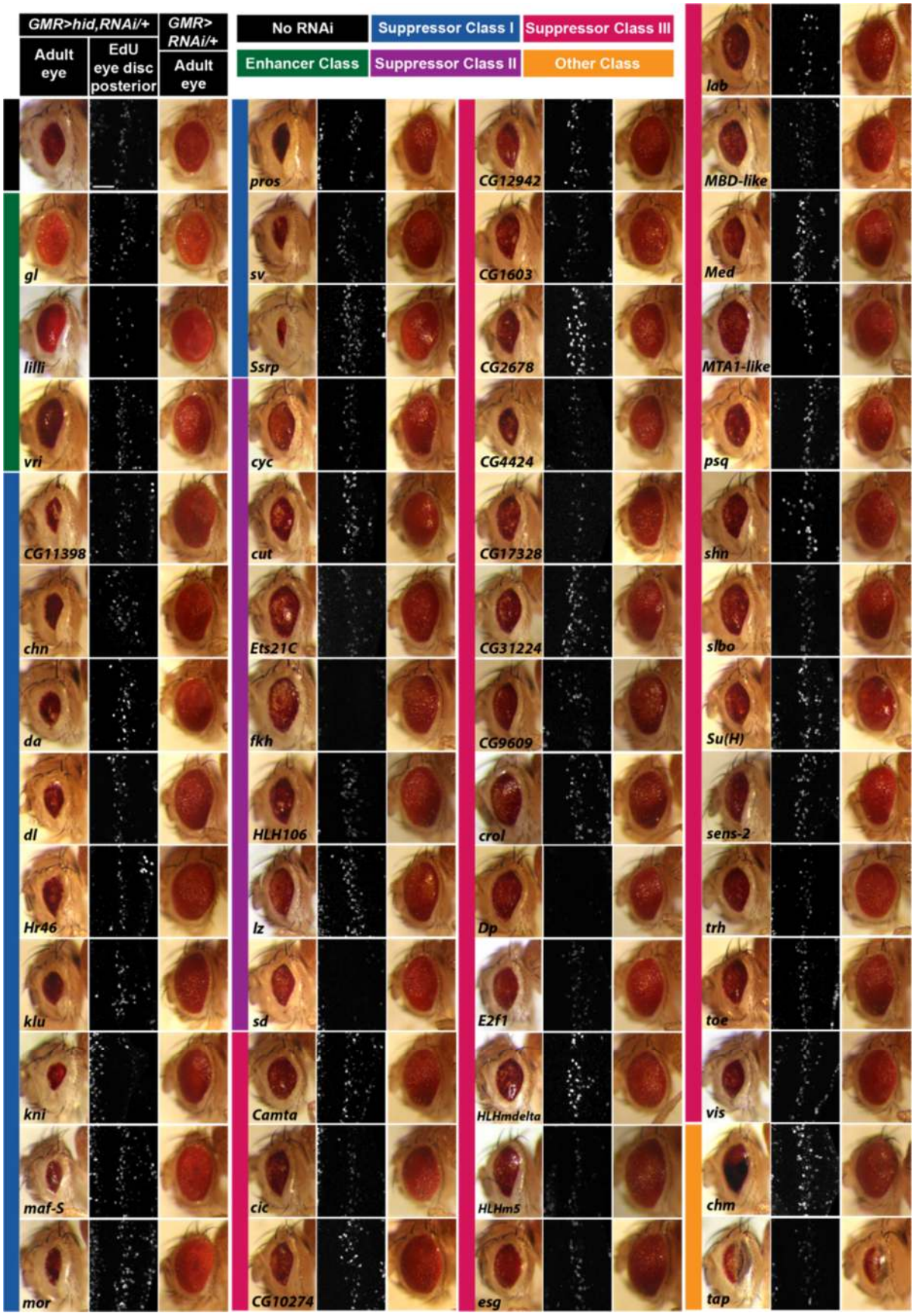
GMR>hid,RNAi/+
Adult eye
EdU eye disc posterior
GMR> RNAi/+
Adult eye
No RNAi
Suppressor Class I
Suppressor Class III
Enhancer Class
Suppressor Class II
Other Class
gl
lilli
vri
CG11398
chn
da
dl
Hr46
klu
kni
maf-S
mor
pros
sv
Ssrp
cyc
cut
Ets21C
fkh
HLH106
lz
sd
Camta
cic
CG10274
CG12942
CG1603
CG2678
CG4424
CG17328
CG31224
CG9609
crol
Dp
E2f1
HLHmdelta
HLHm5
esg
lab
MBD-like
Med
MTA1-like
psq
shn
slbo
Su(H)
sens-2
trh
toe
vis
chm
tap

Supp. Figure 4 (related to Fig. 2). 52 RNAi lines caused a change in the *GMR-hid* adult eye phenotype.

Each UAS-RNAi line was crossed to *GMR>hid, Gal4*. For each line, the adult eye phenotype is displayed in the left column, while the EdU staining of the posterior eye disc is displayed in the right column (centered on the compensatory wave; scale bar: 20 μM and magnification is the same throughout; anterior is oriented to the left). Each line was also crossed to *GMR-Gal4* alone (adult eye phenotype in third column). See Table S1 for full gene names and all RNAi lines tested. First row of images represents the "No RNAi" control. Phenotype classes (see text for explanation): Suppressors=green, Enhancer Class I=blue, Enhancer Class II=purple, Enhancer Class III=pink, Other=orange

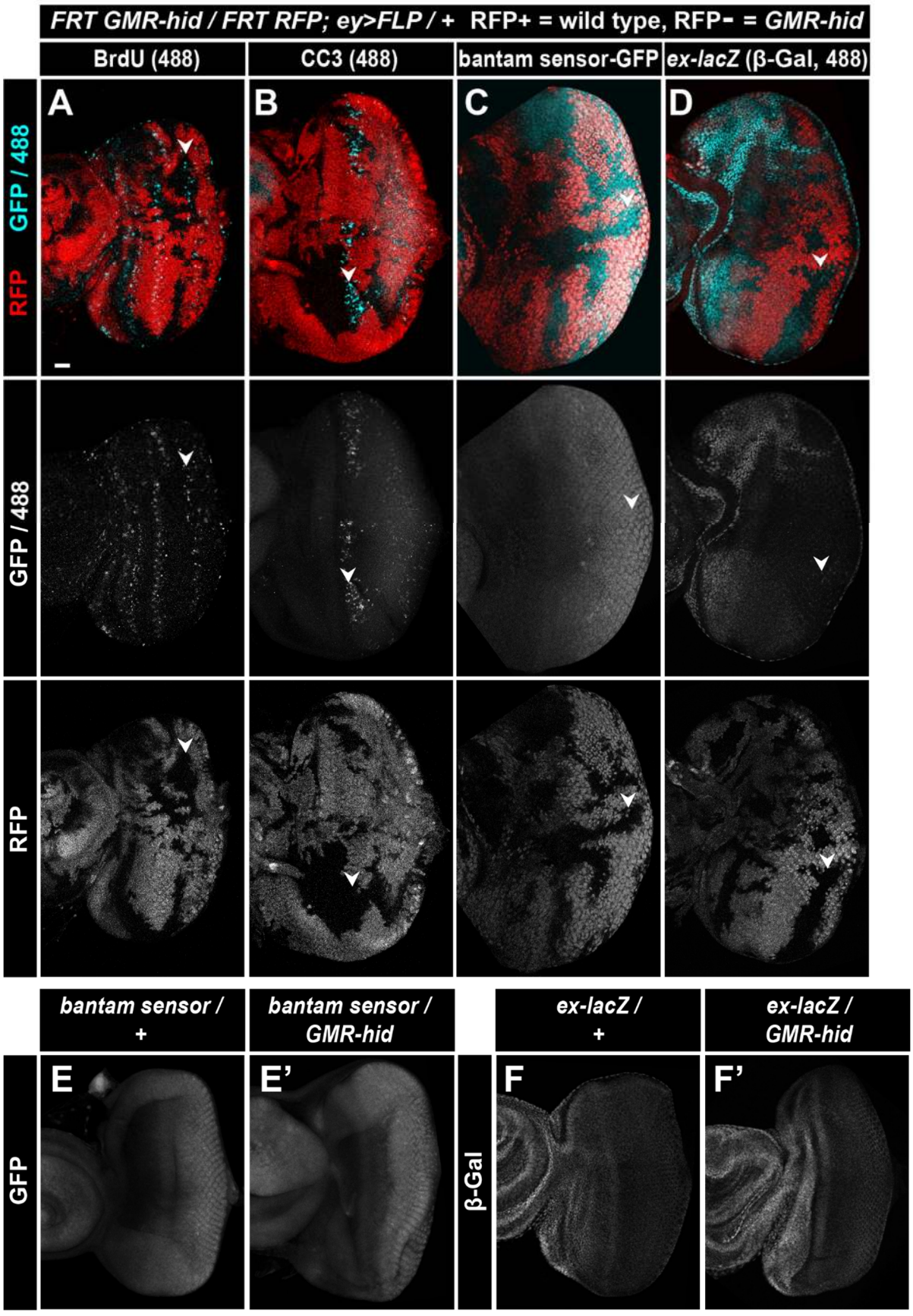
FRT GMR-hid / FRT RFP; ey>FLP / + RFP+ = wild type, RFP- = GMR-hid
BrdU (488)
CC3 (488)
bantam sensor-GFP
ex-lacZ (β-Gal, 488)
A
B
C
D
RFP GFP / 488
GFP / 488
RFP
bantam sensor / +
bantam sensor / GMR-hid
ex-lacZ / +
ex-lacZ / GMR-hid
E
E'
F
F'
GFP
β-Gal

Supp. Figure 5 (related to Fig. 4). A *bantam* sensor and *ex-lacZ* are not induced by *hid* expression in the eye disc.

A-D) *GMR-hid* clones (RFP negative, arrowheads) exhibit CP, marked by EdU (cyan, A), and apoptosis, marked by anti-CC3 staining (cyan, B). *bantam*, measured by the *bantam* sensor-GFP (cyan, C), and *ex-lacZ*, marked by β-Gal (cyan, D), are not induced in *GMR-hid* clones.

E) *bantam* sensor-GFP expression in control (E) and *GMR-hid* (E') eye discs.

F) *ex-lacZ* induction, marked by β-Gal, in control (F) and *GMR-hid* (F') eye discs.

Anterior is oriented to the left. Scale bars: 20 μM.

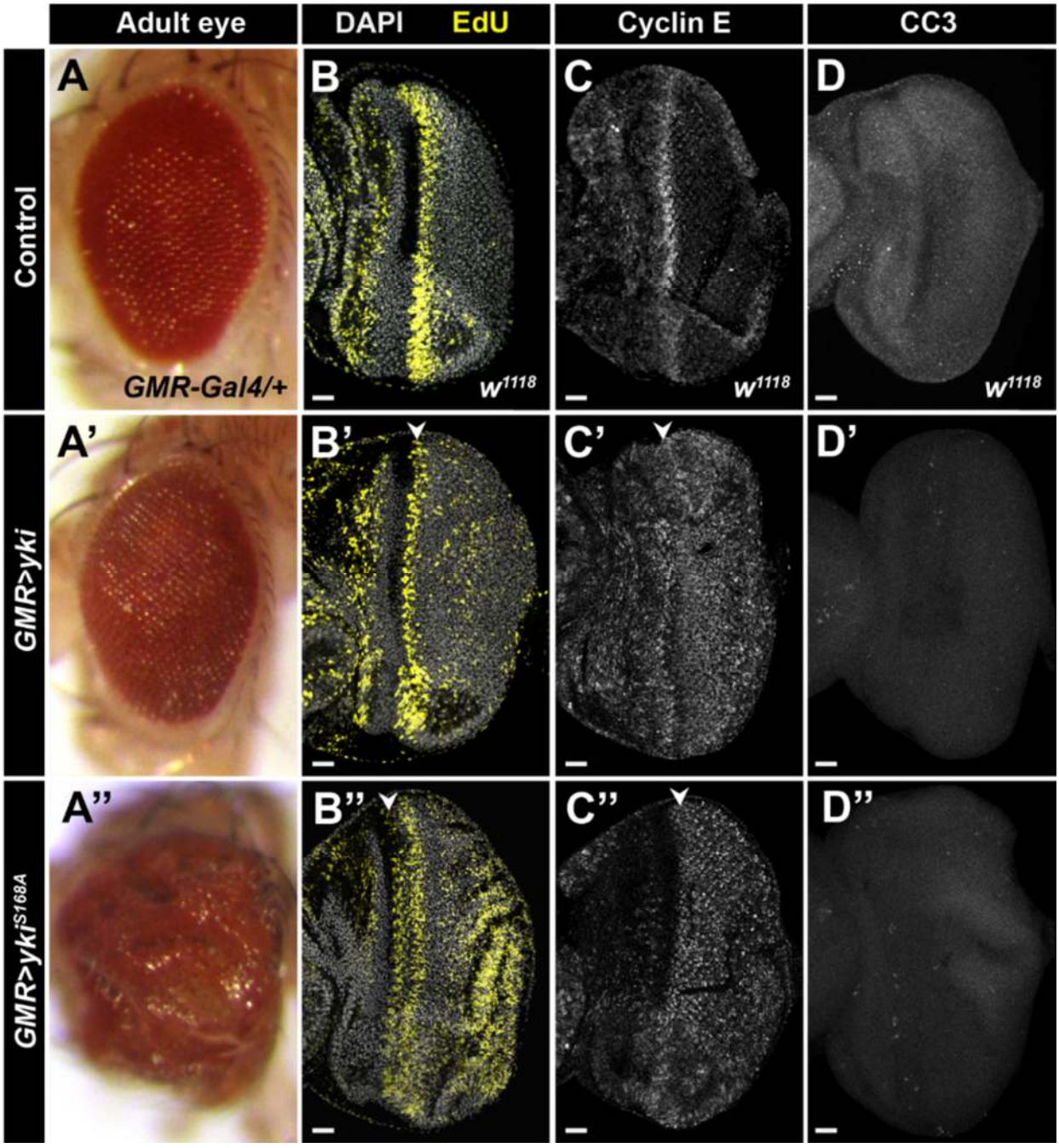

Supp. Figure 6 (related to Fig. 5). Expression of Yki or Yki^{S168A} induces larval and adult eye phenotypes.

A) Adult eyes with *GMR-Gal4* alone (A), with *UAS-Yki* (A'), or with *UAS-Yki^{S168A}* (A'').

B) DAPI staining of nuclei (grey) and EdU staining of S phase cells (yellow) in the indicated genotypes.

C) Staining with anti-Cyclin E antibodies in the indicated genotypes.

D) Staining of apoptotic cells with anti-CC3 antibodies in the indicated genotypes

Anterior is oriented to the left. Scale bars: 20 μM.

Supplementary Experimental Procedures

Fly stocks

RNAi lines used in the screen are listed in supplementary material Table S1. Additional fly stocks used are as follows, with full genotype and Bloomington Stock Center number or providing lab listed in parentheses: ***GMR-hid*** (*P{w[+mC]=GMR-hid}G1*, #5771), ***Tie RNAi*** (*y^1 v^1; P{TRiP.HMJ21428}attP40*, #54005), ***UAS-bsk^{DN}*** (made by K. Matsumoto, obtained from J. Poulton), ***UAS-puc*** (made by A. Martinez Arias, obtained from J. Poulton), ***puc-lacZ*** (*puc-lacZ^{E69}*, made by A. Martinez Arias, obtained from J. Poulton), ***luciferase (luc) RNAi*** (*y^1 v^1; P{TRiP.JF01355}attP2*, #31603), ***Cyclin E RNAi*** (*y^1 v^1; P{TRiP.JF02473}attP2*, #29314), ***UAS-p21*** (I. Hariharan), ***GMR-p21*** (*y^1 w^{1118}; P{GMR-p21.Ex}3/TM3, Sb^1 Ser^1*, #8414), ***sd RNAi-1*** (*y^1 v^1; P{TRiP.JF02514}attP2*, #29352), ***sd RNAi-2*** (*sd (N+C) RNAi*, J. Jiang), ***FRT sd*** (*FRT19A sd^{47m}*, D. Pan), ***FRT RFP*** (*P{Ubi-mRFP.nls}1, w^{1118}, P{neoFRT}19A*, #31416), **FRT GMR-hid; *ey>FLP*** (*P{GMR-hid}SS1, y^1 w* P{neoFRT}19A; P{GAL4-ey.H}SS5, P{UAS-FLP.D}JD2*, #5248), ***Tgi RNAi*** (*y^1 sc* v^1; P{TRiP.HMS00981}attP2*, #34394), ***yki RNAi-1*** (*y^1 v^1; P{TRiP.HMS00041}attP2*, #34067), ***yki RNAi-2*** (*y^1 v^1; P{TRiP.JF03119}attP2*, #31965), ***UAS-dMSTn*** (J. Jiang), ***bantam sensor*** (made by S. Cohen, obtained from T.T. Su), ***ex-lacZ*** (*w*; ex^{e1} P{neoFRT}40A/CyO*, #44249), ***Diap1-lacZ*** (*y^1 w*; P{lacW}Diap1^{j5C8}/TM3, Sb^1*, #12093), ***UAS-yki*** (*y^1 w^*; P{UAS-yki.GFP}4-12-1*, #28815), ***UAS-yki^{S168A}*** (*w*; P{UAS-yki.S168A.V5}attP2*, #28818), ***jub RNAi*** (*y^1 sc* v^1; P{TRiP.HMS00714}attP2*, #32923), ***jub-GFP*** (*w^*; P{jub$^{+t.T:Avic\GFP}$}18A/TM2*, #56806), ***UAS-RokCAT*** (*y^1 w*; P{UAS-Rok.CAT}3.1*, #6669), ***UAS-Cdc42^{DN}*** (*w^*; P{UAS-Cdc42.N17}3*, #6288).

Genotypes for clones are as follows:

sd clones: *FRT19A sd^{47m}/FRT19A Ubi-mRFP.NLS; GMR-hid/+; ey-Gal4, UAS-FLP/+*

GMR-hid clones: *FRT19A GMR-hid/FRT19A Ubi-mRFP.NLS; ey-Gal4, UAS-FLP/+*

GMR-hid clones with *bantam* sensor: *FRT19A GMR-hid/FRT19A Ubi-mRFP.NLS; bantam sensor GFP/+; ey-Gal4, UAS-FLP/+*

GMR-hid clones with *ex-lacZ*: *FRT19A GMR-hid/FRT19A Ubi-mRFP.NLS; ex-lacZ/+; ey-Gal4, UAS-FLP/+*

jub-GFP clones: FRT19A GMR-hid/FRT19A Ubi-mRFP.NLS; jub-GFP/ey-Gal4, UAS-FLP

longGMR-hid transgene construction

To make *longGMR-hid* transgenic flies, the *longGMR* (*LGMR*) enhancer and *hid* ORF were cloned into pMINTGATE, a kind gift from J. Pearson. *LGMR-Gal4* transgene was obtained by PCR amplification from *LGMR-Gal4* flies (Bloomington #8121) with primers white 2161 (forward, GTGTCGCTCGTTGCAGAATA) and Gal4R (reverse, GCCTTGATTCCACTTCTGTCA). The *longGMR* enhancer was then PCR'ed from this fragment with primers LGMRpE F (forward, CACCCAAGCTTTCGCGAGCTCG) and LGMRpE R (reverse, TTTCGCCGGATCTCGACAATAG) and cloned into pENTR/D-TOPO (Invitrogen); pENTR LGMR was then recombined into pMINTGATE using the Gateway LR cloning system (Invitrogen), resulting in pMG LGMR. The *hid* ORF (sequence from BDGP clone AT13267) was synthesized by GenScript with AgeI and SpeI sites for cloning into pMG LGMR, which replaced the *GFP*, but retained the plasmid's SV40 3'UTR. The resulting construct (pMG LGMR hid) was injected by BestGene Inc into the attP40 site to make transgenic flies.

Image quantification

ImageJ (NIH) was used for all quantification. For all statistical measurements, p-values were calculated using the T-test function in Microsoft Excel with two-tailed distribution and two-sample unequal variance.

Measurement of SMW to CP distance

Z-projections were made in ImageJ of EdU staining in control (*GMR>hid, luc RNAi*) or experimental (*GMR>hid, yki*) eye discs. From these images, the physical distance from the anterior edge of the SMW to the anterior edge of the CP wave was measured. To

mitigate confounding effects from preparation artifacts at the dorsal and ventral edges of the disc (e.g. curling over), the distance between the SMW and CP was measured at the approximate midpoint (determined qualitatively) along the D-V axis. In all cases, the farthest distance was measured. Since the CP wave is not entirely synchronous, single EdU^+ cells considerably anterior to other cells in the wave (>10 μM away) were considered anomalies and were not considered in our determination of the anterior CP edge.

Cleaved-Caspase 3 staining

For cleaved Caspase-3 staining quantification, projections of images with anti-CC3 antibody staining were used to calculate total disc area in ImageJ (Huang thresholding to capture entire disc, followed by measurement of total area of particles >100 pixels, which in all cases was one particle, ie the whole disc) and area of CC3 posterior to the furrow (RenyiEntropy thresholding to capture CC3 staining, followed by measurement of total area of particles >3 pixels, which were all cells with CC3 staining). Thresholding was set manually to account for differences in background and signal between samples. Area was used as a measurement rather than total number of $CC3^+$ cells as fragmented cells with pyknotic nuclei could not be unambiguously counted as one or multiple cells. The total area of the disc was used to normalize the area of CC3 staining so that the measurement of CC3 staining is displayed as a percent of total disc area.

Diap-lacZ / β-Gal staining

β-Gal staining from discs with *Diap-lacZ* expression was quantified by calculating the ratio of average intensity of staining posterior and anterior to the furrow. For posterior measurements, a selection containing at least 50 undifferentiated cells (identified by their location apical to the glial cells) in a single slice was made posterior to the furrow. This selection specifically did not include any glial, peripodial, margin, or pre-furrow nuclei, which could confound our measurements. DAPI staining was used to create a ROI containing nuclei. β-Gal fluorescence intensity was then measured in this nuclear ROI. A similar measurement was made with cells anterior to the furrow to normalize differences

in staining between samples. The ratios of average nuclear β-Gal intensity in posterior versus anterior disc cells were used to compare genotypes.

Cyclin E staining

Because staining with anti-Cyclin E antibodies is variable throughout the posterior of eye discs, presumably due to differences in Cyclin E protein accumulation, in each disc we measured the average Cyclin E staining intensity for undifferentiated cells, where differences between genotypes appeared greatest. Since fluorescence from glial, peripodial, or photoreceptor cells could confound our measurements, we gated for undifferentiated cells by applying a mask of Yan staining to Z-stacks of Cyclin E staining. A maximum projection was generated from each gated Cyclin E Z-stack. The resulting image of Cyclin E staining in undifferentiated cells was thresholded using cells with high Cyclin E levels in the SMW as a reference point for Cyclin E positive cells. Since nuclei could not be separated in Z-projected images, area was used as a proxy for cell number. The area of Cyclin E positive cells posterior to the SMW was normalized to the area of Cyclin E positive cells within the SMW. The measurements displayed in Figure 4 and used for quantification are a ratio of post-SMW versus SMW Cyclin E staining area. We considered that the SMW Cyclin E area itself might be different between genotypes, especially considering that Hid expression disrupts the SMW. Therefore, we also measured the area of Cyclin E positive cells posterior to the SMW as a percentage of the total posterior area, based on projections of Yan staining. Statistical comparisons of percent of total posterior disc area with Cyclin E staining for each genotype gave similar significant P-values as our post-SMW versus SMW ratios. We chose to display the post-SMW versus SMW ratios in our results as we feel these measurements better account for differences in staining efficiency than post-SMW area alone.

Table S1.

Click here to Download Table S1